Infrared antenna measurement of the spatial coherence function

Brian Slovick,* Jeffrey Bean, Lou Florence, Guy Zummo, and Glenn Boreman

University of Central Florida, CREOL – The College of Optics and Photonics, 4000 Central Florida Blvd., Orlando, Florida 32816, USA
**bslovick@creol.ucf.edu*

Abstract: The degree of coherence of a partially coherent monochromatic optical field is measured with a dual-dipole phased-array antenna coupled to a metal-oxide-metal tunnel diode detector. For a two-element phased-array, the degree of coherence is a measure of the correlation of electric fields received by the antennas as a function of the element separation. To extract the coherence function from the measured antenna response, a calibration method is developed to remove propagation loss and device nonuniformity. Measurements at 10.6 μm are substantiated by electromagnetic simulations and compared to the result derived from the Van Cittert-Zernike theorem.

OCIS codes: (030.1640) Coherence; (040.3060) Infrared; (110.5100) Phased-array imaging systems.

References and links

1. J. Bean, B. Tiwari, G. Szakmany, G. Bernstein, P. Fay, and W. Porod, "Antenna length and polarization response of antenna-coupled MOM diode infrared detectors," Infrared Phys. Technol. **53**(3), 182–185 (2010).
2. B. A. Slovick, J. A. Bean, P. M. Krenz, and G. D. Boreman, "Directional control of infrared antenna-coupled tunnel diodes," Opt. Express **18**(20), 20960–20967 (2010).
3. J. Wen, S. Romanov, and U. Peschel, "Excitation of plasmonic gap waveguides by nanoantennas," Opt. Express **17**(8), 5925–5932 (2009).
4. P. M. Krenz, R. L. Olmon, B. A. Lail, M. B. Raschke, and G. D. Boreman, "Near-field measurement of infrared coplanar strip transmission line attenuation and propagation constants," Opt. Express **18**(21), 21678–21686 (2010).
5. J. W. Goodman, *Statistical Optics*, (John Wiley & Sons, New York, 1985).
6. A. R. Thompson, J. M. Moran, and G. W. Swenson, *Interferometry and synthesis in radio astronomy*, (John Wiley & Sons, New York, 2001).
7. M. A. Johnson, A. L. Betz, and C. H. Townes, "10-μm heterodyne stellar interferometer," Phys. Rev. Lett. **33**(27), 1617–1620 (1974).
8. S. Brustlein, L. Del Rio, A. Tonello, L. Delage, F. Reynaud, H. Herrmann, and W. Sohler, "Laboratory demonstration of an infrared-to-visible up-conversion interferometer for spatial coherence analysis," Phys. Rev. Lett. **100**(15), 153903 (2008).
9. C. Middlebrook, M. Roggemann, G. Boreman, N. Subotic, K. Cooper, W. Buller, W. Yang, and J. Alda, "Measurement of the Mutual Coherence Function of an Incoherent Infrared Field with a Gold Nano-wire Dipole Antenna Array," Int. J. Infrared Millim. Waves **29**(2), 179–187 (2008).
10. P. M. Krenz, B. A. Lail, and G. D. Boreman, "Calibration of lead-line response contribution in measured radiation patterns of IR dipole arrays," IEEE J. Sel. Top. Quant. **17**(1), 218–221 (2010).
11. L. Mandel, and E. Wolf, *Optical Coherence and Quantum Optics*, (Cambridge Press, New York, 1995).
12. J. Ginn, B. Lail, D. Shelton, J. Tharp, W. Folks, and G. Boreman, "Characterizing Infrared Frequency Selective Surfaces on Dispersive Media," ACES J. **22**, 184–188 (2007).
13. A. Sanchez, C. F. Davis, Jr., K. C. Liu, and A. Javan, "The MOM tunneling diode: theoretical estimate of its performance at microwave and infrared frequencies," J. Appl. Phys. **49**(10), 5270–5277 (1978).
14. I. Codreanu, F. González, and G. Boreman, "Detection Mechanisms in microstrip antenna-coupled infrared detectors," Infrared Phys. Technol. **44**(3), 155–163 (2003).
15. P. M. Krenz, R. L. Olmon, B. A. Lail, M. B. Raschke, and G. D. Boreman, "Near-field measurement of infrared coplanar strip transmission line attenuation and propagation constants," Opt. Express **18**(21), 21678–21686 (2010).
16. J. A. Bean, B. A. Slovick, and G. D. Boreman, "Influence of substrate configuration on the angular response pattern of infrared antennas," Opt. Express **18**(21), 21705–21713 (2010).
17. J. S. Huang, T. Feichtner, P. Biagioni, and B. Hecht, "Impedance matching and emission properties of nanoantennas in an optical nanocircuit," Nano Lett. **9**(5), 1897–1902 (2009).
18. C. Fumeaux, M. Gritz, I. Codreanu, W. Schaich, F. González, and G. Boreman, "Measurement of resonant lengths of infrared dipole antennas," Infrared Phys. Technol. **41**(5), 271–281 (2000).

#142613 - $15.00 USD Received 14 Feb 2011; revised 5 Mar 2011; accepted 7 Mar 2011; published 15 Mar 2011

19. B. Slovick, J. Bean, and G. Boreman, "Angular resolution improvement of infrared phased-array antennas," IEEE Antenn. Wireless Propag. Lett. (to be published in 2011).
20. J. A. Bean, B. Tiwari, G. H. Bernstein, P. Fay, and W. Porod, "Long wave infrared detection using dipole antenna-coupled metal–oxide–metal diodes," J. Vac. Sci. Technol. B **27**(1), 11 (2009).
21. J. Bean, A. Weeks, and G. Boreman, "Performance optimization of antenna-coupled Al/AlO_X/Pt tunnel diode infrared detectors," IEEE J. Quantum Electron. **47**(1), 126–135 (2011).
22. J. W. Goodman, *Introduction to Fourier Optics*, (Roberts & Co., Englewood, Colorado 2005).
23. P. Krenz, B. Slovick, J. Bean, and G. Boreman, "Alignment procedures for radiation pattern measurements of antenna-coupled infrared detectors," Opt. Eng. **49**(3), 033607 (2010).

1. Introduction

Infrared (IR) phased-array antennas when coupled to metal-oxide-metal (MOM) tunnel diodes provide a versatile detection mechanism that allows for simultaneous determination of the polarization, wavelength, and angle of origin of an optical source [1,2]. A common design includes a pair of dipole antennas coupled to a MOM diode through a coplanar strip (CPS) transmission line [3,4]. Determination of the angle of origin is possible by varying the position of the MOM diode along the transmission line connecting the antenna elements [2].

In a logical extension of this method, a phased-array can be used to assess the degree of coherence of a partially coherent field, and through the Van Cittert-Zernike theorem, deduce the spatial intensity distribution of the source [5]. This approach has been implemented at microwave frequencies by radio astronomers since the 1950s. Image reconstruction of astronomical sources is achieved via inverse Fourier transformation of the complex electric fields measured at spatially separated observatories [6]. Methods of measuring the coherence function in the IR include intensity interferometry with heterodyne detection [7], IR-to-visible up-conversion interferometry [8], and antenna-coupled microbolometric detection [9]. The latter approach is inherently limited by the distributed impedance that is characteristic of bolometers with poor TCR contrast [10]. Moreover, previous configurations had the antenna geometry fixed while varying the diameter of the spatially incoherent source.

We present a method in which the spatially incoherent source is fixed while the separation of the antenna elements is varied. In this configuration, the degree of spatial coherence is a measure of the correlation of electric fields received by the antennas as a function of their separation. This scheme is analogous to Young's double-slit arrangement with the pinholes replaced by dipole antennas and the far-field transformation of light from the pinholes to the observation screen regarded as propagation of antenna currents along a CPS transmission line.

2. Method

The traditional setup for measuring the degree of coherence of a partially coherent field consists of a pair of pinholes and an observation screen [5]. For a two-element phased array, the separation of the dipole antennas is analogous to the pinhole separation and the MOM diode represents a point on-axis in the observation screen. Figure 1 contains electron micrographs of the two-element phased-array antenna and MOM diode. The dipole antennas are separated by a distance *L* and the MOM diode is located at the center of the array.

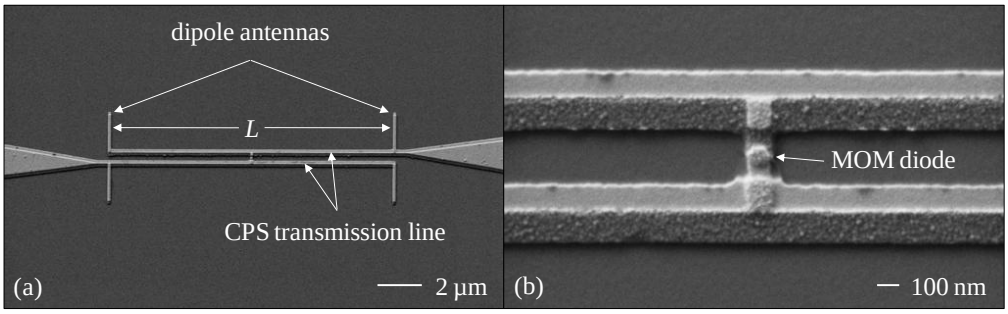

Fig. 1. Electron micrographs of the phased-array antenna (a) and MOM diode (b).

#142613 - $15.00 USD Received 14 Feb 2011; revised 5 Mar 2011; accepted 7 Mar 2011; published 15 Mar 2011

With CPS propagation loss included, the two-source interference law for partially coherent light is [5]

$$I(L) = \exp(-\alpha L)[I_1 + I_2 + 2\sqrt{I_1 I_2}\,\mathrm{Re}\,\gamma(L)], \tag{1}$$

where I_1 and I_2 are the squares of the CPS current amplitudes, α is the attenuation constant of the CPS, and $\gamma(L)$ is the complex coherence function of the partially coherent source. Consider a circular lens uniformly illuminated with monochromatic spatially incoherent light. From the Van Cittert-Zernike theorem, the coherence function on-axis is real with a magnitude [11]

$$|\gamma(L)| = 2\left|\frac{J_1(\pi L / \lambda F/\#)}{(\pi L / \lambda F/\#)}\right|, \tag{2}$$

where *F/#* is the focal ratio of the lens, λ is the wavelength, and $J_1(x)$ is a Bessel function of the first kind. If the CPS currents have equal magnitudes, $I_1 = I_2 = I_0$ and Eq. (1) simplifies to

$$I(L) = 2I_0 \exp(-\alpha L)[1 + |\gamma(L)|]. \tag{3}$$

Equation (3) represents the measured antenna response, which is generally subject to device non-uniformity through the parameter I_0. Determination of the coherence function from Eq. (3) thus requires knowledge of the CPS attenuation constant and device uniformity. Therefore, a calibration method is required for extraction of the coherence function from the measured response. To this end, consider the antenna response under coherent illumination with $\gamma(L)$=1,

$$I_C(L) = 4I_{0,C} \exp(-\alpha L), \tag{4}$$

where the letter *C* denotes coherent illumination. For partially coherent illumination (denoted by the letter *P*), the coherence function can take any value between zero and unity,

$$I_P(L) = 2I_{0,P} \exp(-\alpha L)[1 + |\gamma(L)|]. \tag{5}$$

By eliminating the exponential with Eq. (4), we can solve for the coherence function in Eq. (5) to obtain

$$|\gamma(L)| = 2\frac{I_{0,C} I_P(L)}{I_{0,P} I_C(L)} - 1. \tag{6}$$

The ratio $I_{0,C}/I_{0,P}$ can be determined by measuring the single dipole response (L = 0) under coherent and partially coherent illumination ($I_C(0)$ and $I_P(0)$, respectively). Taking the ratio of these quantities yields

$$\frac{I_C(0)}{I_P(0)} = \frac{2I_{0,C}}{I_{0,P}[1+\gamma(0)]} = \frac{2I_{0,C}}{I_{0,P}[1+1]} = \frac{I_{0,C}}{I_{0,P}}. \tag{7}$$

Inserting the ratio from Eq. (7) into Eq. (6), the coherence function can be written as

$$|\gamma(L)| = 2\frac{I_C(0) I_P(L)}{I_P(0) I_C(L)} - 1. \tag{8}$$

To verify that the quantity in Eq. (8) is independent of device non-uniformity, first consider the ratio $I_C(0)/I_P(0)$. Since the electric fields are perfectly correlated at the location of a single dipole, the ratio $I_C(0)/I_P(0)$ is simply a measure of the power ratio of the two sources. Now, the quantity $I_P(L)/I_C(L)$ depends on the power ratio of the sources as well as the degree of coherence at the antenna separation L. Therefore, their combined ratio in Eq. (8) can depend only on the degree of coherence. To summarize, by measuring the responses of a single dipole and two-element phased-array under coherent and partially coherent illumination, the coherence function can be determined independently of propagation loss and

#142613 - $15.00 USD Received 14 Feb 2011; revised 5 Mar 2011; accepted 7 Mar 2011; published 15 Mar 2011

device non-uniformity. In this calibration method, we are effectively setting equal the device responses for coherent illumination.

3. Simulation and design

Numerical simulations are performed in Ansys High Frequency Structure Simulator (HFSS), a commercial electromagnetic finite element solver. In HFSS, the antenna structure is modeled in detail, including the overlapping metals from the shadow evaporation (see section 4) as well as the intermediate aluminum-oxide layer. Material properties, including refractive index and film thickness, are measured using a J.A. Woollam Infrared Variable-Angle Spectroscopic Ellipsometer (IR-VASE) and incorporated into the electromagnetic models to increase the accuracy of the simulations [12].

When excited with infrared radiation, MOM diodes exhibit a non-linear *I*-*V* characteristic caused by the tunneling of electrons through the insulator layer [13]. At zero bias, the dc component of the rectified current is proportional to the optical power dissipated in the oxide layer [14]. In HFSS, a quantity proportional to the rectified current is computed as the power loss density integrated over the aluminum-oxide volume [2]. From Eq. (8), the degree of coherence can be calculated by evaluating the antenna response for coherent and partially coherent illumination. To simulate coherent *F*/8 illumination (see section 4) for determination of $I_C(L)$, the antenna is excited in HFSS with a Gaussian beam of waist w_0 = 115 μm and wavelength 10.6 μm (28.3 THz). The power dissipated in the oxide layer is then calculated as a function of the antenna separation. For the partially coherent case, we calculate the power dissipated for *F*/1 Gaussian beam illumination at each angle of incidence in an *F*/1 cone (54° full angle) and evaluate the sum to obtain $I_P(L)$. In this respect, by adhering to the principle of superposition of powers (or intensities), we are assuming a spatially incoherent source. The coherence function is calculated by taking the ratio of the coherent and partially coherent responses in the manner prescribed by Eq. (8).

Design considerations for a two-element phased array include the substrate configuration, antenna length and spacing, and CPS gap width. To reduce inhomogeneities in the dielectric environment and hence reduce propagation loss in the CPS, the devices are fabricated on a low-index (n = 1.55) quarter-wavelength dielectric layer above a ground plane [15,16]. The dielectric is a 1.7 μm layer of benzocyclobutene (BCB), a low loss insulator (k = 0.015) at 10.6 μm. The antenna length and CPS separation are chosen to optimize power transfer from free-space radiation to confined modes in the CPS [2,17]. From a parametric analysis, the optimal antenna length and CPS gap width are 4 μm and 470 nm center-to-center, respectively. This antenna length corresponds to one half-wavelength of 10.6 μm radiation at a BCB-air interface [18]. The dipole antenna and CPS widths are 100 nm and 260 nm, respectively. The maximum antenna separation is chosen to minimize propagation loss in the CPS and to include the first zero of the coherence function, which from Eq. (2), occurs for an antenna spacing

$$L_0 = 1.22\lambda F/\#. \tag{9}$$

A recent investigation of the influence of propagation loss on the angular response patterns of multiple-element IR phased-arrays demonstrates that antenna elements with separations greater than 24 μm do not contribute to the measured response [19]. Anticipating a similar degree of propagation loss and with knowledge of the condition for minimum visibility, we choose an *F*/1 spatially incoherent source and vary the antenna separation between zero and 18 μm.

4. Fabrication and measurement

Antenna-coupled MOM diodes are fabricated using electron beam lithography, electron beam evaporation, and vacuum chamber oxidation [1,20]. By performing the metal depositions at opposing angles, the two metals overlap beneath a suspended bridge of undercut electron beam resist (Fig. 1(b)). Aluminum and platinum are chosen for their work function contrast and high conductivity in the IR [21]. The thickness of each metal layer is 30 nm. Prior to the

#142613 - $15.00 USD Received 14 Feb 2011; revised 5 Mar 2011; accepted 7 Mar 2011; published 15 Mar 2011

Pt layer deposition, oxygen is released into the vacuum chamber at 100 mTorr, allowing the Al to grow a 10-15 Å thick native oxide. The lead lines, bond pads, antenna-coupled CPS, and diode are deposited without breaking vacuum in the evaporation chamber.

An illustration of the measurement configuration is shown in Fig. 2. A 10.6 μm CO_2 laser is mechanically chopped at 1.5 kHz in the focal plane of a ZnSe lens. The diverging radiation is passed through a rotating piece of sandblasted BaF_2 and focused by an *F*/1 BaF_2 lens placed directly behind the diffuser. In this configuration, the Fraunhofer diffraction pattern of the spatially incoherent field is generated in the focal plane of the *F*/1 lens [22].

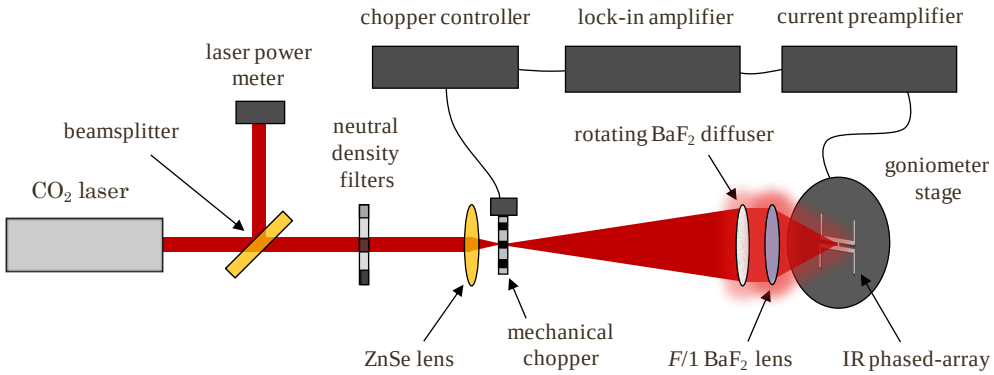

Fig. 2. Experimental configuration for spatial coherence measurements. Radiation passing through the BaF_2 diffuser undergoes diffuse refraction to form a spatially incoherent field. The Fraunhofer diffraction pattern is generated in the focal plane of the *F*/1 lens. For calibration, the diffuser and *F*/1 lens are replaced with a collimating lens and *F*/8 objective, respectively.

The phased-array antenna is mounted to a five-axis goniometer located in the focal plane of the *F*/1 lens [23]. The rectified current from the MOM diode is passed through an external current preamplifier and monitored with a lock-in amplifier that is referenced to the frequency of the mechanical chopper. Temporal fluctuations in the laser power are accounted for by normalizing the measured current to the reference power. Measurements are conducted without external applied bias and with a laser irradiance of approximately 10 $W \cdot cm^{-2}$. The measured response to radiation polarized perpendicular to the dipoles is nearly equal to the Johnson noise, which indicates that the dc lead line and thermal contributions are negligible.

One can characterize the coherence properties of the diffuser by comparing the surface roughness to the average displacement of the diffuser between consecutive measurements. For example, if the chopper frequency is 1.5 kHz and the average diffuser rotational frequency is 3 Hz, there are 500 measurements during one rotational cycle of the diffuser. The displacement between measurements by a point midway between the center and edge of a 5 cm diameter diffuser is approximately $0.5\pi(5\text{ cm})/500 \approx 160$ μm. From contact profilometry measurements of the BaF_2 surface, depth variations of 1-2 λ are separated on average by 10 λ, or around 100 μm. Since the average roughness separation is less than the displacement between measurements, the phase distribution across the diffuser can be regarded as random between measurement cycles, thus substantiating the use of a spatially incoherent source in the simulations.

Determination of the coherence function from Eq. (8) requires measurement of the coherent and partially coherent responses. For the coherent response $I_C(L)$, each device is measured under *F*/8 illumination with the diffuser removed. A high *F*/# lens is less susceptible to alignment errors and generates a large spot size compared to the antenna separation. The latter condition is essential when comparisons are made to the extended uniform image of a partially coherent source. The *F*/8 optics are then removed and replaced by the diffuser and *F*/1 transform lens. The antenna response is then measured to obtain $I_P(L)$. From Eq. (8), the coherence function is calculated by normalizing to the single dipole ratio $I_C(0)/I_P(0)$.

#142613 - $15.00 USD Received 14 Feb 2011; revised 5 Mar 2011; accepted 7 Mar 2011; published 15 Mar 2011

Figure 3 shows the measured coherence function compared with the HFSS simulation and analytical result from the Van Cittert-Zernike theorem (Eq. (2)). Error bars represent one standard deviation from the mean of measurements conducted with diffuser frequencies of 1.5, 3, 4.5, and 6 Hz. Agreement between simulation and measurement is very good, while moderate discrepancies are apparent between the measurement and the Van Cittert-Zernike result. In all three cases, the minimum in the coherence function occurs for antenna separations between 12 and 13 μm, in agreement with Eq. (9). For this antenna separation, the electrics fields received by the antennas are uncorrelated in the sense that CPS current amplitudes generated by these antennas will not exhibit interference. Instead, the principle of superposition applies to the CPS current intensities. Deviations from the Van Cittert-Zernike theorem are attributed to mutual interactions between the reradiated fields of the dipole antennas and variations in the effective impedance of the CPS as a function of the antenna separation. Both effects are apparent in simulations as deviations from the exponential behavior predicted by Eq. (4). If the aluminum-oxide layer is replaced with a different material (e.g., SiO_2), the oscillations in the simulated coherence function shift spatially, inferring that these features are related to impedance mismatches between the CPS and diode.

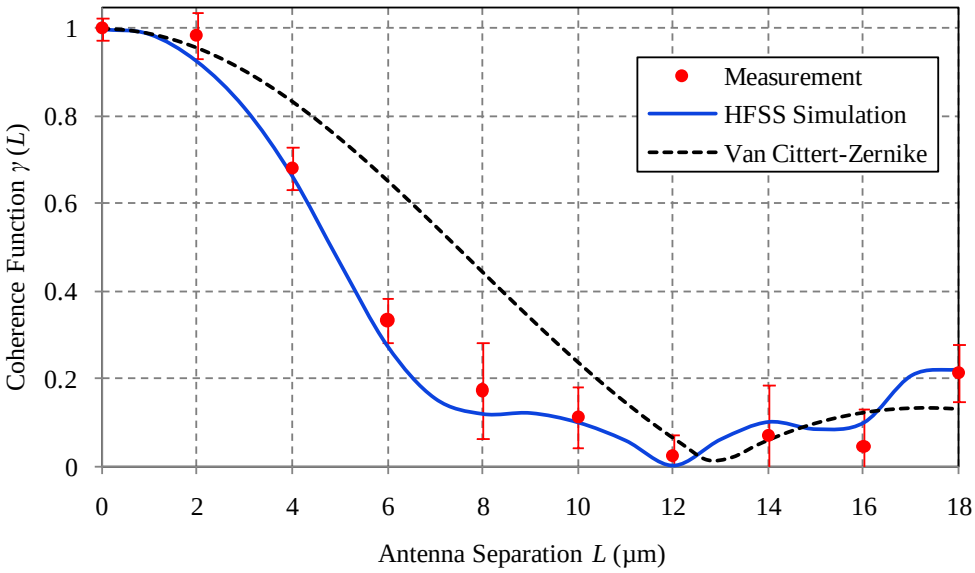

Fig. 3. Measured and simulated spatial coherence function versus antenna separation for a two-element phased-array. The standard result from the Van Cittert-Zernike theorem is also shown.

5. Conclusions

In analogy to Young's double-slit experiment, a phased-array antenna can be used to assess the degree of coherence of a spatially extended monochromatic optical field. For a two-element array, the degree of coherence is a measure of the correlation of electric fields received by the antennas as a function of the element separation. In general, phased-array antennas coupled to MOM diodes and CPS transmission lines are subject to propagation loss and device non-uniformity. By properly calibrating the antenna response with coherent illumination and normalizing with respect to the single dipole response, the coherence function can be extracted from the measured antenna response under partially coherent illumination. Electromagnetic simulations and the standard result from the Van Cittert-Zernike theorem are confirmed by measurements with a 10.6 μm CO_2 laser and a partially coherent F/1 source.

#142613 - $15.00 USD Received 14 Feb 2011; revised 5 Mar 2011; accepted 7 Mar 2011; published 15 Mar 2011